Journal of Sol-Gel Science and Technology
https://doi.org/10.1007/s10971-021-05683-y

ORIGINAL PAPER: FUNCTIONAL COATINGS, THIN FILMS AND MEMBRANES (INCLUDING DEPOSITION TECHNIQUES)

The deep investigation of structural and opto-electrical properties of Yb_2O_3 thin films and fabrication of Al/Yb_2O_3/p-Si (MIS) Schottky barrier diode

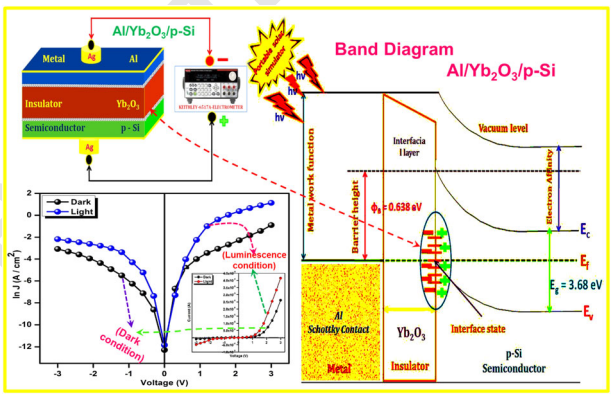
A. Panneerselvam[1] · K. S. Mohan[2] · R. Marnadu[3] · J. Chandrasekaran[3]

Received: 30 March 2021 / Accepted: 30 October 2021
© Springer Science+Business Media, LLC, part of Springer Nature 2021

Abstract

The present research explores the fabrication of a metal insulator semiconductor Schottky barrier diode (SBD) with rare earth metal oxide (Yb_2O_3) thin films as insulators that are effectively developed on a large scale using the low-cost jet nebulizer spray pyrolysis technique (JNSP). The Yb_2O_3 thin films are deposited at various substrate temperatures (350 °C–550 °C) to ascertain its influence on the characteristic properties of the material. The structural, morphological and opto-electrical properties are investigated using various characterization techniques. Here, X-ray diffraction (XRD) analysis revealed the single crystalline cubic crystal structure of Yb_2O_3 thin films. Field emission scanning electron microscope (FESEM) images show the presence of uniformly distributed cage and globular like structures spread over the entire surface of the Yb_2O_3 films. The elemental composition study demonstrates the presence of Yb and O. The optical direct energy band gap of Yb_2O_3 thin films have been analyzed through UV-Visible spectra. Current – voltage measurements were analyzed in dark and light conditions for the Al/Yb_2O_3/p-Si structured Schottky barrier diodes (SBDs) which are fabricated with interfacial layers at different substrate temperatures. Further, the functionality of the SBDs was tested at different temperatures ranging from 30 °C to 150 °C. The experimental results of all SBDs indicate a linear reduction in the ideality factor (n) up to 2.537 and 2.059 with a slight increase in the effective barrier height (Φ_B) of 0.789 eV& 0.638 in dark and light conditions, respectively. The SBD fabricated at 550 °C recorded good performance, which will be suitable for thermal dependent electronic device applications.

Graphical Abstract



✉ K. S. Mohan
mohanm.scm.phil@gmail.com

[1] Department of Physics, Vivekanandha College of Engineering for Women (Autonomous), Elayampalayam, Tiruchengode, Namakkal 637 205 Tamil Nadu, India

[2] Department of Physics, Nandha Engineering College (Autonomous), Erode 638 052 Tamil Nadu, India

[3] Department of Physics, Sri Ramakrishna Mission Vidyalaya College of Arts and Science (Autonomous), Coimbatore 641020 Tamil Nadu, India

UNCORRECTED PROOF

Keywords Yb_2O_3 thin films · Spray pyrolysis · Globular-like structure · I-V characteristics · Schottky barrier diodes

1 Introduction

In modern times, rare earth materials have been widely used in a variety of applications, particularly in multi-layer structures such as metal-insulator-semiconductor (MIS), metal-insulator-metal (MIM), metal-oxide-semiconductor (MOS), and metal-polymer-semiconductor (MPS). They also attract many researchers due to their large bandgap, wide breakdown region, and high saturation velocity that is well suited for high-power electronic device applications such as field-effect transistors, metal-insulator semiconductors, and high-electron-mobility transistors [1, 2]. Due to its promising properties in optoelectronic/microelectronic device applications involving diode, transistor, capacitor, power conversion systems, and high-speed switching devices [3–5], the MIS structure was of great interest for many years. They function as a diode or rectifier, allowing carriers to be transmitted at forwarding bias and preventing reverse bias [6, 7]. The MIS Schottky diode is researched by many research groups with different insulating layers, such as Al_2O_3, HfO_2, etc. having been investigated. [8]. In general, the thin interfacial layer plays a significant role in altering the electrical properties of the Schottky diode from MIS.

The rare earth sesquioxide Yb_2O_3 is a cubic refractory material with bandgap energy >4 eV [9, 10]. It is used as sintering additives, with high refractory quality, making it ideal for higher temperatures than standard oxides, such as Al_2O_3 and MgO. In fact, at relatively low temperatures, these latter oxides form amorphous liquid phases. Yb_2O_3 thin films have been identified as an efficient additive with higher oxidation resistance and high-temperature strength retention to improve thermal diffusivity and conductivity [11]. Compared with other materials, Yb_2O_3 has excellent dielectric properties with excellent thermodynamic stability and Si substratum interface properties [12]. Because of its excellent comprehensive properties, large conduction band offset with Si, low-frequency dispersion, and low hysteresis voltage, Yb_2O_3 films are considered as an ideal candidate in the production of SBDs [13]. Nowadays, Yb_2O_3 films have been extensively used in sensors, capacitors, and resistive random access memory applications in addition to diode fabrication [14]. In such applications, work into the substrate temperature-dependent phase transformation of Yb_2O_3 thin films would be very important to improve the rectification parameters for SBDs. It is also necessary to characterize and obtain a correlation between the structural, morphological, optical, and electrical properties of thin films of Yb_2O_3 as a function of the substrate's temperature.

Many researchers have worked to understand the electrical characteristics of Schottky barrier diodes (SBDs) and their applications in sensing and optoelectronics using various metallization strategies. Rajagopal Reddy et al. investigated the electronic parameters and interface state properties of a Yb/p-InP Schottky diode by studying the current-voltage characteristics (IV), capacitance-voltage frequency (CVf), and conductance voltage frequency. The barrier height and ideality factor were found to be 0.68 eV and 1.24 eV, respectively. Under forward bias conditions, the ohmic and space charge limited conduction mechanisms were identified at low and higher voltages. Jyothi et al. studied the structural changes of Au/Yb contacts to p-type GaN using X-ray diffraction, X-ray photoemission spectroscopy, and atomic force microscopy. A barrier height of 0.84 eV was obtained for the as-deposited Au-Yb/p-type GaN Schottky diode. The barrier height decreased after annealing at temperatures above 500 °C. The decrease in the barrier height could be due to the evolution of gallide phases, which generate Ga vacancies. Marnadu et al. investigated the electrical properties of as-deposited Cu/Wo_3/p-Si Schottky diodes and showed that the ideality factor of 2.89 and corresponding barrier height of 0.71 eV were recorded for higher substrate temperature. Vivek et al. fabricated Cu/MoO_3/p-Si SBDs obtained at a T_{sub} of 500 °C that exhibited much better rectification behavior and a lower ideality factor of 2.84 as seen from I-V characteristics [15–18]. However, compared to these results, rare earth metal oxides enhance the electrical properties and hence the present investigation was attempted with Yb_2O_3 as an insulating layer.

Moreover, many Schottky contact components such as Al, Cu, Ag, Te, and Au are used in various SBDs and these show promising rectification properties with relatively low current density for leakage. Because of the presence of an interfacial insulator layer and the interface states situated at the MIS interface [19], the effective barrier height is believed to be bias-dependent. Interestingly, the lower work function of the Schottky contact plays a vital role in fabricating MIS structure SBDs that influence diode parameters such as ideality factor (n), barrier height (Φ_B), reverse leakage current density (Jo), and resistance (Rs) [20]. Due to low resistance and smaller band gap size, Al is an optimal Schottky contact with high work efficiency compared with other materials.

UNCORRECTED PROOF

Silicon is an indirect bandgap semiconductor for which the charge carrier lifetime is greater, and the current amplification is also high, resulting in better diode properties. There are several methods of shaping thin Yb_2O_3 films, such as spray pyrolysis, laser ablation, spin coating, sputtering, electron beam evaporation, and atomic layer deposition (ALD) [21–25]. The jet nebulizer spray pyrolysis (JNSP) technique, however, is the most important method for thin-film preparation and is also widely adopted in material science industries. JNSP has many advantages, such as cost-effective and simple experimental setup, high throughput, greater homogeneity, wide area coating with good product purity, high speed, and fewer impurities which aids in manufacturing smooth, ultra-thin films with a controllable thickness within a limited time period [26]. In addition, core problems such as surface morphology and stoichiometry can be regulated in the JNSP technique. Furthermore, we can also alter the deposition parameters such as substrate temperature, air pressure, and solution volume during film deposition.

In the current study, Yb_2O_3 thin films have been prepared using JNSP technique with different substrate temperatures, such as 350 °C, 400 °C, 450 °C, 500 °C, and 550 °C. The influences on the Yb_2O_3 thin film such as structural, morphological, and optoelectrical characteristics are discussed. Subsequently, Al/Yb_2O_3/p-Si (MIS) Schottky diodes are cast using the deposited Yb_2O_3 thin films as an insulating layer between Al/p-Si interfaces. Herewith, key diode parameters such as n, Φ_B, and saturation current (I_0) are extracted by using I–V characteristics of the diodes at various substrate temperatures of Yb_2O_3 thin films.

2 Experimental and characterization details

2.1 Yb_2O_3 thin film preparation

In this present work, chemical reagents such as ytterbium (III) chloride hexahydrate ($YbCl_3.6H_2O$) with 99.99% purity were purchased from Sigma Aldrich. To prepare high-quality Yb_2O_3 thin films, 0.2 mol of $YbCl_3.6H_2O$ was dissolved in 10 ml deionized water and stirred for 45 min. at 350 K using a magnetic stirrer. Before coating, all the substrates were cleaned using isopropyl alcohol (IPA) and soap solution, and acetone separately. Subsequently, the prepared solution was deposited on well-cleaned glass substrates at different temperatures, viz. 350 °C, 400 °C, 450 °C, 500 °C, and 550 °C on an area of $2 \times 2.5\ cm^2$ on the substrate. The deposition parameters, such as pressure and volume of the solution, the diameter of the nozzle, and time relevant to the JNSP route were optimized for Yb_2O_3 films, as summarized in Table 1 [27]. The chemical reaction when deionized water is used as solvent at similar substrate temperatures can be written as

$$2YbCl_3.6H_2O \rightarrow \frac{\Delta}{(350\,^{\circ}C - 550\,^{\circ}C)} \rightarrow Yb_2O_3 + 6HCl \uparrow + 3H_2O \uparrow \quad (1)$$

2.2 Silicon wafer cleaning process

The Al/Yb_2O_3/p-Si Schottky diodes were prepared by using a single side polished surface p-type float zone silicon (100) wafer (1 × 1 cm size) with 0–60 Ω surface resistivity and 250 ± 25 µm thickness. The Si wafer cleaning process is an important step in the fabrication of this MIS diode since Si wafers have many impurities, including dust, grease, metallic impurities, and organic residues. The existence of the surface impurities and organic residues can also influence the performance of the MIS diode.

It is essential to synthesis an ultra-pure substrate surface for preparing the diode. Hence, the following cleaning steps were used to prepare the Si wafer. The wafer was first dipped in piranha solution ($H_2SO_4 + H_2O_2$) in the ratio of 3:1 for 25 min to remove grease impurities with the help of deionized water. It was then soaked in a solution of (HF + H_2O taken in a ratio of 10:1) to eliminate the native oxide layer (SiO_2) from the Si substrate. The silicon wafer was completely immersed in de-ionized water after each cleaning process.

2.3 Fabrication of Al/Yb_2O_3/p-Si SBD_S

The prepared Yb_2O_3 solution was sprayed on the well-cleaned p-type Si wafers using a JNSP route at different substrate temperatures, viz. 350 °C, 400 °C, 450 °C, 500 °C, and 550 °C. The aluminum (Al) metal contact was deposited on Yb_2O_3/p-Si using dc-magnetron

Table 1 Optimized deposition parameters of Yb_2O_3 thin films

Parameters	Values
Diameter of the nozzle	0.6 mm
Distance between substrate and nozzle	6 cm
Pressure maintained	3.2 kg cm^{-2}
Deposition flow rate	0.6 ml min^{-1}
Time of spray	20 min
Substrate Temperature	350 °C, 400 °C, 450 °C, 500 °C, and 550 °C

UNCORRECTED PROOF

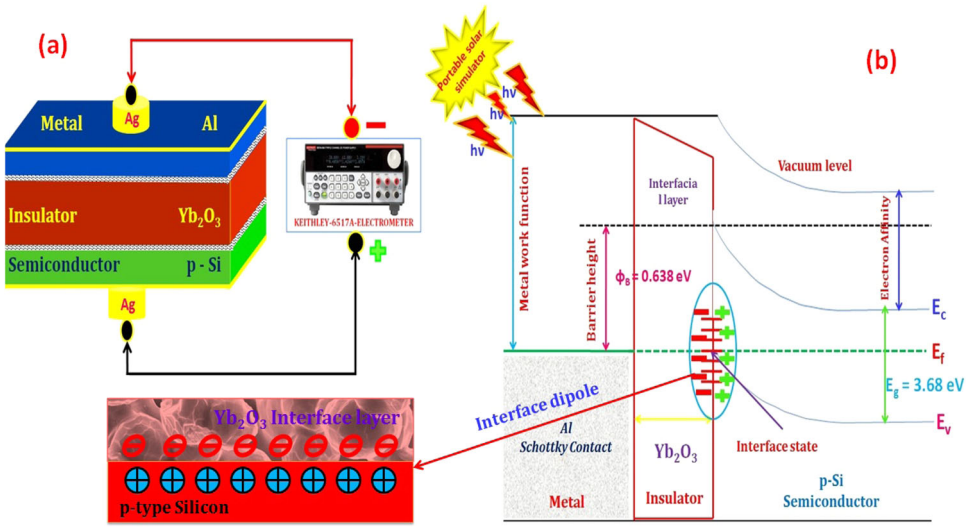


Fig. 1 **a** Schematic sketch of MIS SBDs. **b** Energy level band diagram of the Al/Yb_2O_3/p-Si Schottky barrier diode

sputtering (HIND high vacuum PS 2000) with standard pressure of 6 millibars. A non-rectifying junction referred to as an ohmic contact was made by applying silver (Ag) paste on both sides of the fabricated Al/Yb2O3/p-Si SBDs and then dried at room temperature for 6 hours. The Ag paste provides stronger adhesion properties, improved electrical contact, low sheet resistance (>0.02 Ω/cm), and solderability. The schematic diagram and energy level diagram of the Al/Yb_2O_3/p-Si diodes are shown in Fig. 1 (a, b).

2.4 Characterization techniques

First, a stylus profilometer (Mitutoyo SJ-301) with a diamond needle was used to test the thickness of the coated Yb_2O_3 thin films. The XRD patterns of the Yb_2O_3 thin films were analyzed with a Rigaku Miniflex-II ($CuK\alpha_1$ radiation with $\lambda = 1.5418$ Å) within the 2θ range of 10−80°. Atomic force microscopy (model: 5100 Pico LE) and field emission scanning electron microscopy (Zeiss Sigma model: FEI quanta 250) were used to analyze the surface and morphological behavior of Yb_2O_3 films. The presence of elements such as Yb and O was determined by energy dispersive X-ray analysis (EDX). The optical properties were studied using UV–vis spectroscopy (JASCO, model: V-770PC). Photoluminescence (PL) spectra were captured at 300 K using a spectrofluorometer (JASCO, model: FP-8300) in the wavelength range 200–750 nm. Finally, the electrical properties of the prepared thin films were determined using a two-probe approach at various temperatures (30−150 °C). A Keithley electro-meter (Model: 6517B) was used to study the current-voltage (I–V) characteristics of the fabricated Al/Yb_2O_3/p-Si diode.

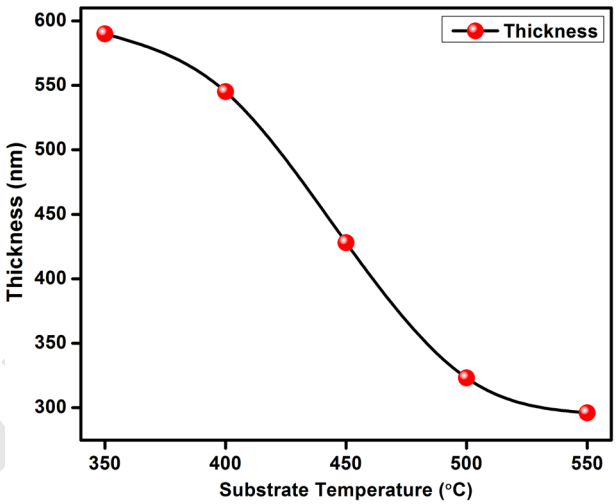


Fig. 2 Thickness variation of the Yb_2O_3 thin films for different substrate temperature

3 Results and discussion

3.1 Thickness variation of the Yb_2O_3 films

Variations in the thickness of the Yb_2O_3 films with increasing substrate temperature are shown in Fig. 2, and indicate that the thickness decreases from 590 to 296 nm when the substrate temperature increases from 350 °C to 550 °C. These data show that the JNSP technique plays an important role in controlling the film thickness, with increasing substrate temperature leading to a corresponding decrease in Yb_2O_3 film thickness [28].

3.2 XRD analysis

Figure 3(a–e) shows the XRD pattern of the spray deposited Yb_2O_3 thin films at various substrate

UNCORRECTED

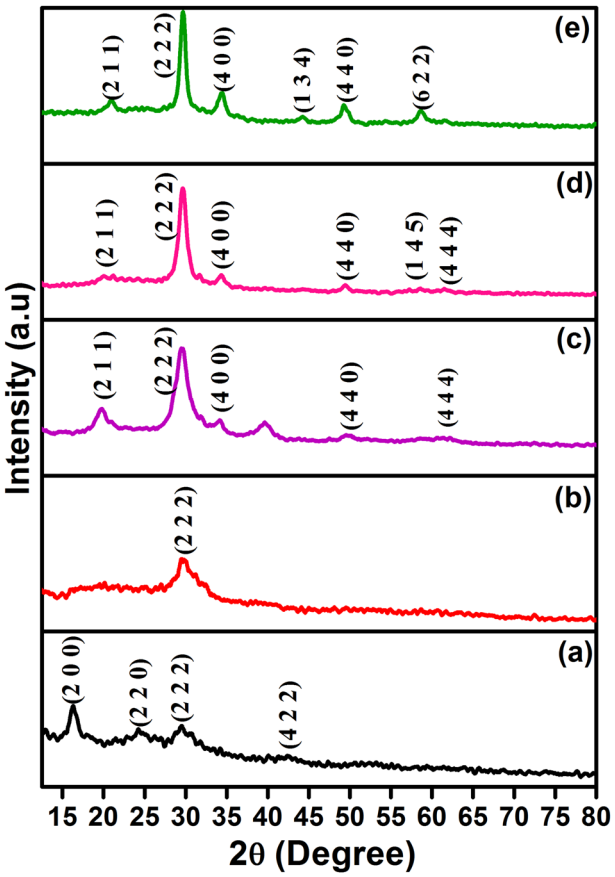


Fig. 3 XRD pattern of the Yb_2O_3 thin films for different T_{sub} values of **a** 350 °C, **b** 400 °C, **c** 450 °C, **d** 500 °C, and **e** 550 °C

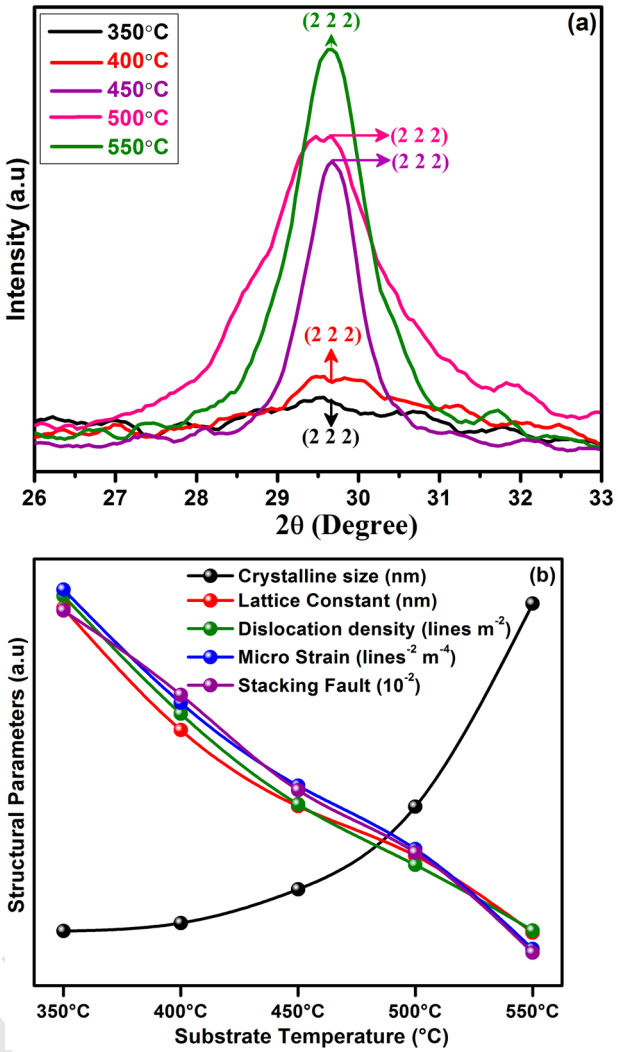


Fig. 4 **a** XRD Peak position of the Yb_2O_3 films for different substrate temperatures. **b** Structural Parameters of Yb_2O_3 thin films with different substrate temperatures

temperatures. The intensity of the diffraction peaks increases with increasing substrate temperature with the maximum intensity relative to the other films observed with a substrate temperature of 550 °C. The Yb_2O_3 films belong to the cubic crystal system having space group Ia $\bar{3}$(206), which is indexed and matched with the JCPDS cards no.65–5792 and 65–3173 respectively [27]. The composition of c-Yb_2O_3 is confirmed by the diffraction angle [2θ (°)] of the peaks at 16.31, 20.27, 24.48, 29.55, 34.11, 42.57, 44.33, 49.22, 57.90, 58.67, and 61.53° and their corresponding (h k l) planes (200), (211), (220), (222), (400), (422), (134), (440), (145), (622), and (444), respectively [29]. There is no phase change observed in Yb_2O_3 films with increasing substrate temperature. However, a slight distortion occurs in the structure of the films, which is attributed to changes in the lattice parameter and crystallite size. A favored orientation along the (222) plane is observed at higher substrate temperatures [30]. As the temperature of the substrate increases, the predominant peak intensity gradually increases as is clearly shown in Fig. 4a. These results imply that the higher substrate temperature plays a vital role in film formation along the (222) direction. However, in some planes, the preferred orientation of crystallites can influence peak height. If more crystallites orient along one particular direction, usually the corresponding peak height will increase. The average crystallite size (D) of the Yb_2O_3 film is calculated using Scherrer's formula which is given in Eq. (2) [31]. The Lattice constant (a), dislocation density (δ), microstrain (ε), and stacking fault (SF) are obtained by using the following Eqs. (3–6) and the calculated values are summarized in Table 2.

$$\text{Crystallite Size} \quad (D) = \frac{(0.89)\lambda}{\beta\cos\theta} \tag{2}$$

$$\text{Lattice constant}\,(a) = d \times \sqrt{(h^2 + k^2 + l^2)} \tag{3}$$

$$\text{Dislocation Density} \quad (\delta) = \frac{1}{D^2} \tag{4}$$

UNCORRECTED

Table 2 Calculated Structural parameters of spray-coated Yb_2O_3 thin films for different substrate temperature

Substrate temperature (°C)	2θ (°)	(h k l)	*d* (Å)	FWHM (in Rad)	*a* (nm)	*D* (nm)	$\delta \times 10^{16}$ lines m^{-2}	$\varepsilon \times 10^{-2}$ lines^{-2} m^{-4}	SF × 10^{-2}
350 °C	16.31	$(2\ 0\ 0)_c$	5.434	0.0137	1.0868	10.20	0.9606	0.3399	0.931
	24.49	$(2\ 2\ 0)_c$	3.635	0.0206	1.0281	6.892	2.1065	0.5035	1.122
	29.49	$(2\ 2\ 2)_c$	3.029	0.0206	1.0491	6.963	2.0628	0.4982	1.023
	42.57	$(4\ 2\ 2)_c$	2.123	0.0412	1.0403	3.613	7.6599	0.9601	1.676
400 °C	29.65	$(2\ 2\ 2)_c$	3.013	0.0199	1.0441	7.197	1.9304	0.4819	1.032
450 °C	29.38	$(2\ 2\ 2)_c$	3.040	0.0133	1.0532	10.75	0.8656	0.3228	0.337
	34.12	$(4\ 0\ 0)_c$	2.628	0.0137	1.0511	10.56	0.8959	0.3284	0.627
	49.34	$(4\ 4\ 0)_c$	1.841	0.0240	1.0391	6.351	2.4791	0.5462	0.898
	61.64	$(4\ 4\ 4)_c$	1.505	0.0325	1.0425	4.976	4.0386	0.6971	1.132
500 °C	20.28	$(2\ 1\ 1)_c$	4.381	0.0143	1.0728	9.825	1.0359	0.3531	0.856
	29.56	$(2\ 2\ 2)_c$	3.022	0.0100	1.0469	14.32	0.4876	0.2422	0.493
	34.28	$(4\ 0\ 0)_c$	2.616	0.0103	1.0464	14.09	0.5035	0.2462	0.469
	49.45	$(4\ 4\ 0)_c$	1.843	0.0107	1.0426	14.32	0.4942	0.2439	0.399
	57.90	$(1\ 4\ 5)_c$	1.593	0.0212	1.0321	7.474	1.7900	0.4641	0.721
	61.53	$(4\ 4\ 4)_c$	1.507	0.0206	1.0441	7.836	1.6285	0.4427	0.675
550 °C	21.00	$(2\ 1\ 1)_c$	4.231	0.0103	1.0364	13.72	0.5331	0.2533	0.605
	29.76	$(2\ 2\ 2)_c$	3.002	0.0052	1.0401	27.87	0.1288	0.1245	0.255
	34.49	$(4\ 0\ 0)_c$	2.601	0.0086	1.0403	16.92	0.3493	0.2050	0.391
	44.33	$(1\ 3\ 4)_c$	2.043	0.0137	1.0419	10.91	0.8408	0.3181	0.543
	49.23	$(4\ 4\ 0)_c$	1.851	0.0052	1.047	29.63	0.1139	0.1171	0.194
	58.68	$(6\ 2\ 2)_c$	1.573	0.0137	1.0437	11.59	0.7449	0.2994	0.462

$$\text{Micro Strain} \qquad (\varepsilon) = \frac{\beta \cos\theta}{4} \tag{5}$$

$$\text{Stacking Fault} \qquad (SF) = \left[\frac{2\pi^2}{45(3\tan\theta)^{\frac{1}{2}}}\right]\beta \tag{6}$$

here, D is the average crystallite size, λ is the wavelength (0.15418 nm) for CuKα, β is the full-width at half maximum of the diffraction peak and θ is the diffraction angle in degrees. The average crystallite size of the Yb_2O_3 films is found to increase with increasing substrate temperature. This result indicates that the substrate temperature improved the crystalline nature of the films. The substrate temperature strongly affects structural parameters such as crystallite size and lattice constants as shown in Fig. 4b. The average crystallite size increased from 7 to 18 nm with increasing substrate temperature [32, 33]. The lattice constant of the films gradually decreases with increasing temperature. The significant narrowing of the peaks indicates the increasing crystallite size with increasing substrate temperature [34]. Maximum crystallite size of 18 nm is observed at a higher substrate temperature of 550 °C as indicated by the smaller FWHM. The crystallization levels of the films are good, even though slight defects are present in the film, that is confirmed from the calculated dislocation density (δ). Dislocation density has been observed to decrease with a rise in crystallite size, that is attributed to a decrease in the occurrence of grain boundaries as the crystallite size increases with increasing substrate temperature. The lowest average dislocation density value (0.4518×10^{16}) is recorded at a higher substrate temperature of 550 °C. At higher substrate temperatures, the calculated values of stacking fault (sf) and microstrain (ε) are found to decrease due to the reduction in the interplanar spacing, and thus decrease the stacking fault probability in the Yb_2O_3 thin films. The values are summarized in Table 2. Overall, the XRD results provide clear evidence for the formation of the Yb_2O_3 films [34].

3.3 Surface morphology

FESEM was used to analyze the surface structure and grain organization of the deposited Yb_2O_3 films at different substrate temperatures. When Yb_2O_3 is deposited at different substrate temperatures from 350 °C to 550 °C, the surface morphology of the films is observed to vary, confirming the dependence of surface morphology on the

UNCORRECTED PROOF

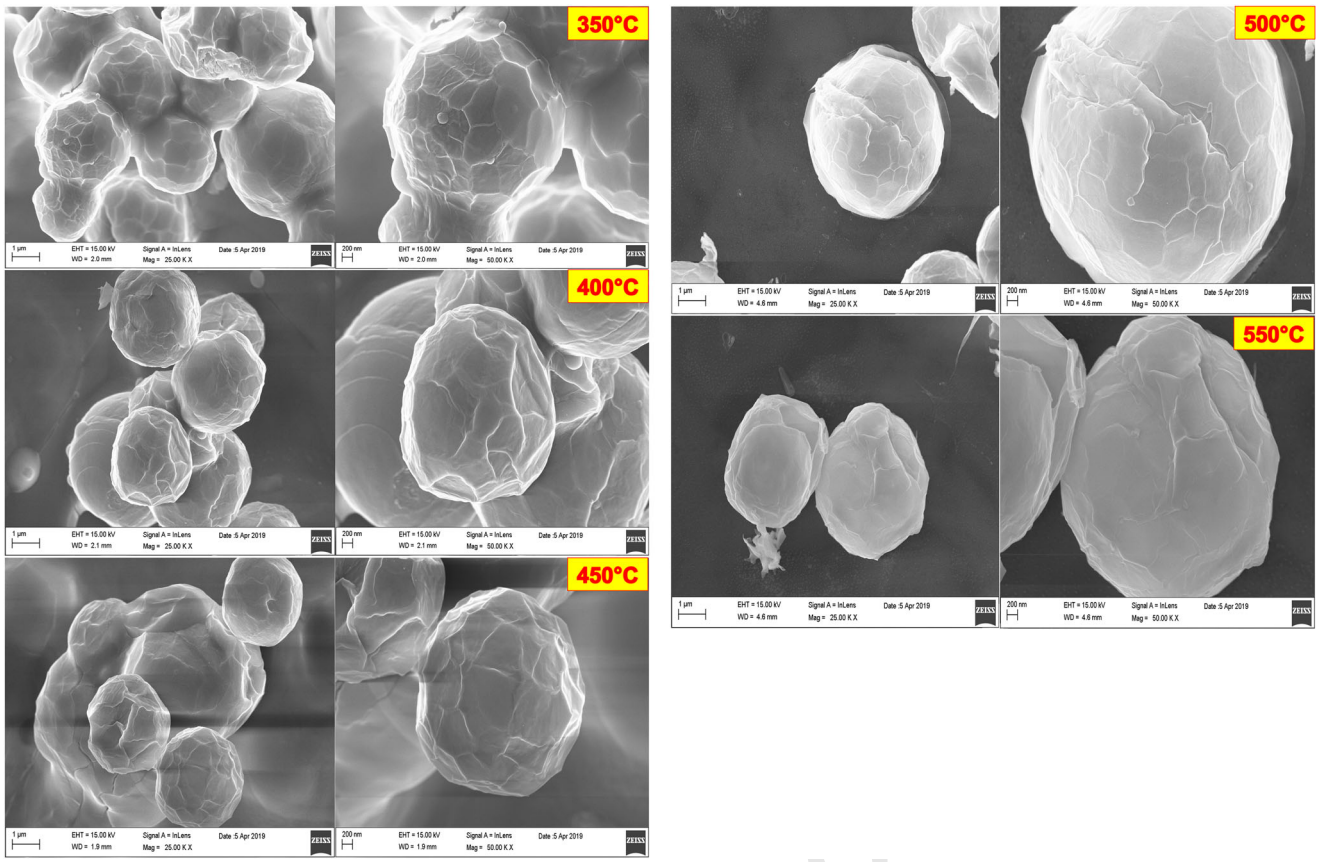


Fig. 5 FE – SEM images of Yb_2O_3 thin films developed by JNSP root at the different substrate temperature

substrate temperature as shown in Fig. 5. The FESEM images reveal that no cracking occurred even during large area scanning. For the Yb_2O_3 films deposited at 350 °C −450 °C, randomly oriented cage-like structures are observed. Because of the oxidation of Yb atoms, the higher substrate temperature favors the fast and defect-free growth of grains. As the temperature of the substrate increases, the cage-like structure turns into a globular shape. Interestingly, when the substrate temperature is increased from 500 °C to 550 °C, due to the compactness of spray droplets moving towards the substrate, a slight agglomeration is observed on the surface [35]. When the substrate temperature increases from 350 to 550 °C, the crystallite size was found to increase from 7 nm to 18 nm [36].

3.4 Elemental composition

Figure 6 displays the EDX distribution of Yb_2O_3 thin films deposited in the substrate temperature range of 350–550 °C at various substrate temperatures. The observed spectra reveal the presence of expected elements such as Yb and O in the deposited films. The composition data in Table 3 clearly indicate that as the substrate temperature (350 −550 °C) is increased, the Yb:O ratio decreases up to 450 °C and then increases further due to a reduction in the oxygen content. This result indicates an excess of oxygen in the prepared Yb_2O_3 films. The reduction of Yb content at higher substrate temperature increases the film conduction directly [37].

3.5 Surface roughness

AFM is used to evaluate the surface topography of the spray depositedYb_2O_3 thin films at an optimized substrate temperature of 550 °C. Figure 7(a–c) shows the 2D and 3D topographic images from AFM along with the corresponding surface roughness histogram recorded over an area of 1μm x 1μm. The 2D topography image in Fig. 7(a) illustrates the non-uniform distribution and rough surface of the film. The 3D image in Fig. 7(b) clearly indicates that the small particles are aggregated together to build a conical structure with some voids. Figure 7(c) shows the surface roughness histogram from which the average surface roughness (R_a) was calculated to be 5.7 nm and area root mean square (RMS) as 6.1 nm at a substrate temperature of 550 °C [38]. Furthermore, the Yb_2O_3 thin film with a large grain size is expected to show improved

UNCORRECTED PRO

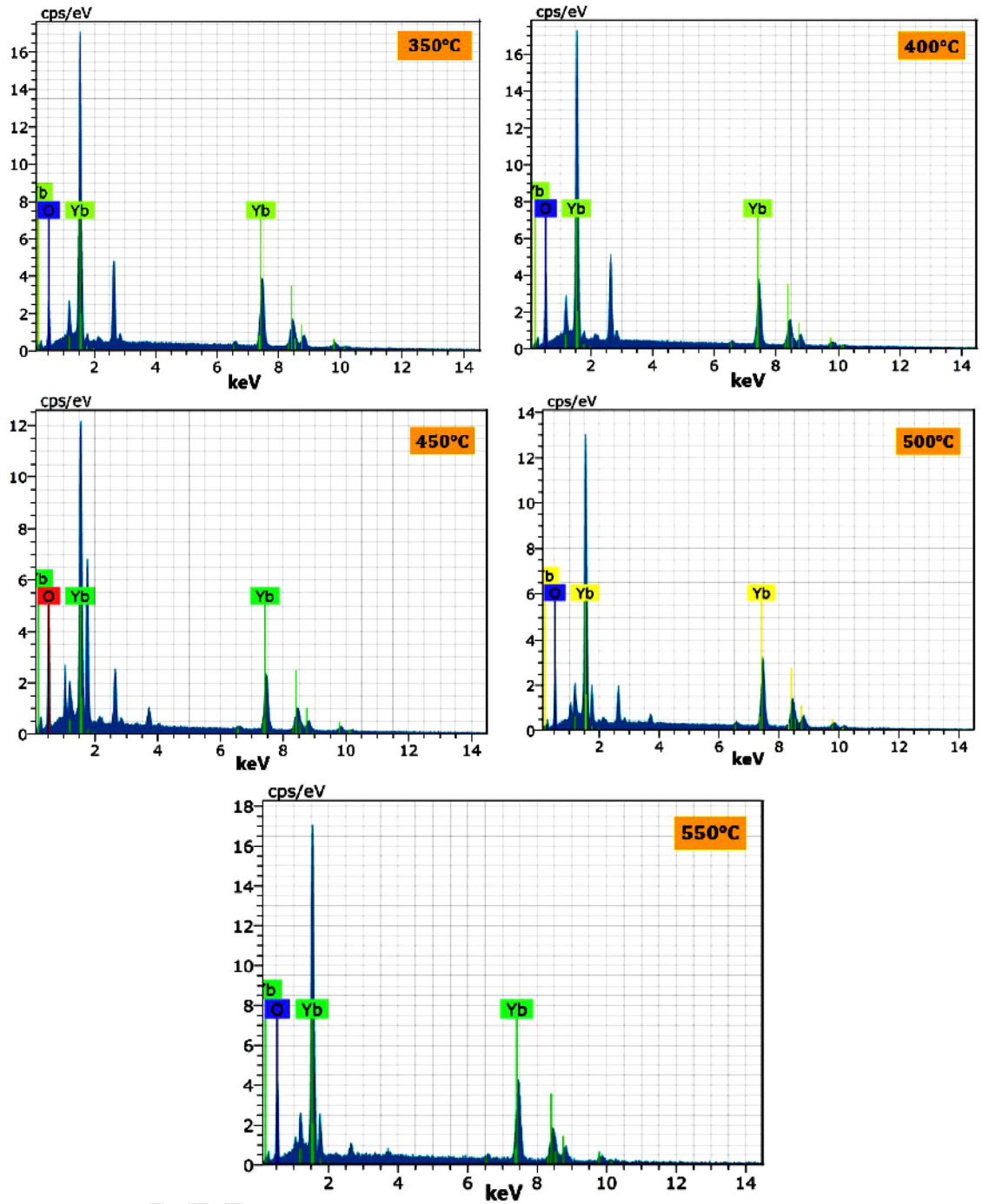


Fig. 6 EDX spectrum of Yb_2O_3 films attained at a different substrate temperature

electrical behavior in the films and subsequently an enhancement in the device performance. Another reason is the reduced surface diffusion of atoms/molecules that resulted in a rough surface. Thus, the morphological variations are in good agreement with results from FESEM and XRD analysis that might lead to better conductivity values in the films, which favors a high-performing MIS structure SBD.

3.6 UV-Vis spectrum

The optical properties of the Yb_2O_3 thin films deposited at various substrate temperatures were investigated by UV–visible spectrometry. Figure 8(a) reveals that the optical absorbance of the films gradually rises in the UV-visible region, decreasing sharply with increasing wavelength and then remains constant. This is consistent with the deep

Table 3 Elemental composition of spray-coated Yb_2O_3 films for various substrate temperatures

Substrate Temperature (°C)	Atomic Ratio (%)	
	Yb	*O*
350	28.71	71.29
400	23.26	76.24
450	14.25	85.75
500	28.99	71.01
550	30.2	69.8

bluish coloration of the thin films. However, the maximum optical absorption of Yb_2O_3 thin films is observed at the higher substrate temperature of 550 °C in the UV region [39, 40]. From the UV–visible spectra, the optical band gap (E_g) values are obtained from the following Eq. 7.

$$\text{Optical band gap} \qquad (\alpha h\nu)^n = A\left(h\nu - E_g\right) \qquad (7)$$

The optical band gap values are determined from Tauc's plot ($(\alpha h\nu)^2$ vs. ($h\nu$)) for Yb_2O_3 films as shown in Fig. 8b. When n is 2, it specifies a directly permitted transition, and the

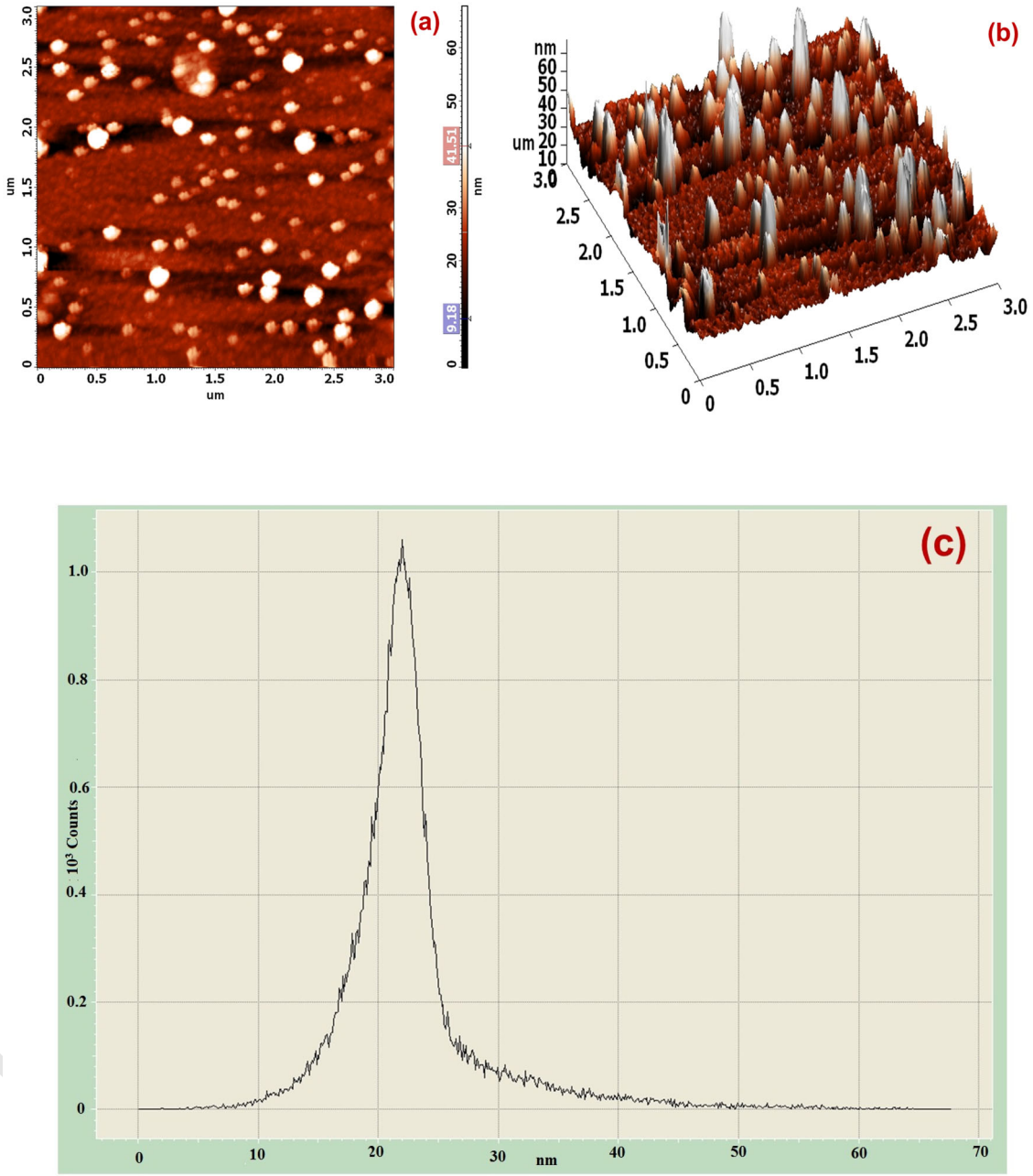


Fig. 7 **a** AFM image of 2D, **b** 3D, **c** Histogram optimized temperature 550 °C of Yb_2O_3 films

intercepts on the X- axis is equivalent to the E_g values. Interestingly, the energy gap values were found to increase from 3.43 to 3.68 eV as the substrate temperature increased from 350 °C to 550 °C. The bandgap values are gradually increased with an increase in the substrate temperature due to the reduction in the film thickness. This leads to the reduction in the leakage current in semiconducting devices such as diodes [41]. The optical parameters such as absorption coefficient (α), extinction coefficient (k), and refractive index (n) are calculated by the following relations 8–10.

$$\text{Absorption Co-efficient} \qquad (\alpha) = \left[\frac{1}{t}\right] \ln\left[\frac{1}{T}\right] \tag{8}$$

$$\text{Extinction Co-efficient} \qquad (k) = \left[\frac{\alpha\lambda}{4\pi}\right] \tag{9}$$

$$\text{Refractive index} \qquad (n) = \frac{1+R}{1-R} \pm \sqrt{\frac{4R}{(1-R)^2} - k^2} \tag{10}$$

where α, T, t, λ, R, and k are the absorption coefficient, transmittance, thickness, wavelength, reflectance, and extinction coefficient, respectively. The absorption coefficient (α) values are found to be reduced with increasing substrate temperature up to 550 °C. Due to the reduced film thickness, the absorption coefficient has a higher value. If the values of $\alpha > 10^5$, there is a maximum possibility for the allowed direct transition. The absorption coefficient slightly decreases with increasing wavelength and remains constant at a higher wavelength. Similarly, the extinction coefficient values are found to be reduced with increasing substrate temperature from 350 to 550 °C, indicating that the films have higher densification and absorb light very well at higher substrate temperatures [42]. In addition, the calculated refractive index (n) varied from 2.79 to 2.86 with increasing substrate temperature. The refractive index (n) recorded a higher value at the substrate temperature of 550 °C. The improved packing density value results in an increasing refractive index. Thus, the observed optical parameters of the Yb_2O_3 films are significantly influenced by the substrate temperature, as illustrated in Table 4 and Fig. 8(c).

3.7 Photoluminescence spectrum

Figure 9 shows the photoluminescence spectra of Yb_2O_3 thin films that were prepared with different substrate temperatures from 350 °C to 550 °C, using an excitation wavelength of 250 nm. It is observed that the peak around 299 nm corresponds to the ultraviolet emission of Yb_2O_3 thin films and consequently the band gaps of the samples are calculated using the formula $E_g = hc/\lambda$. The PL peak intensity was found to be maximum for the sample

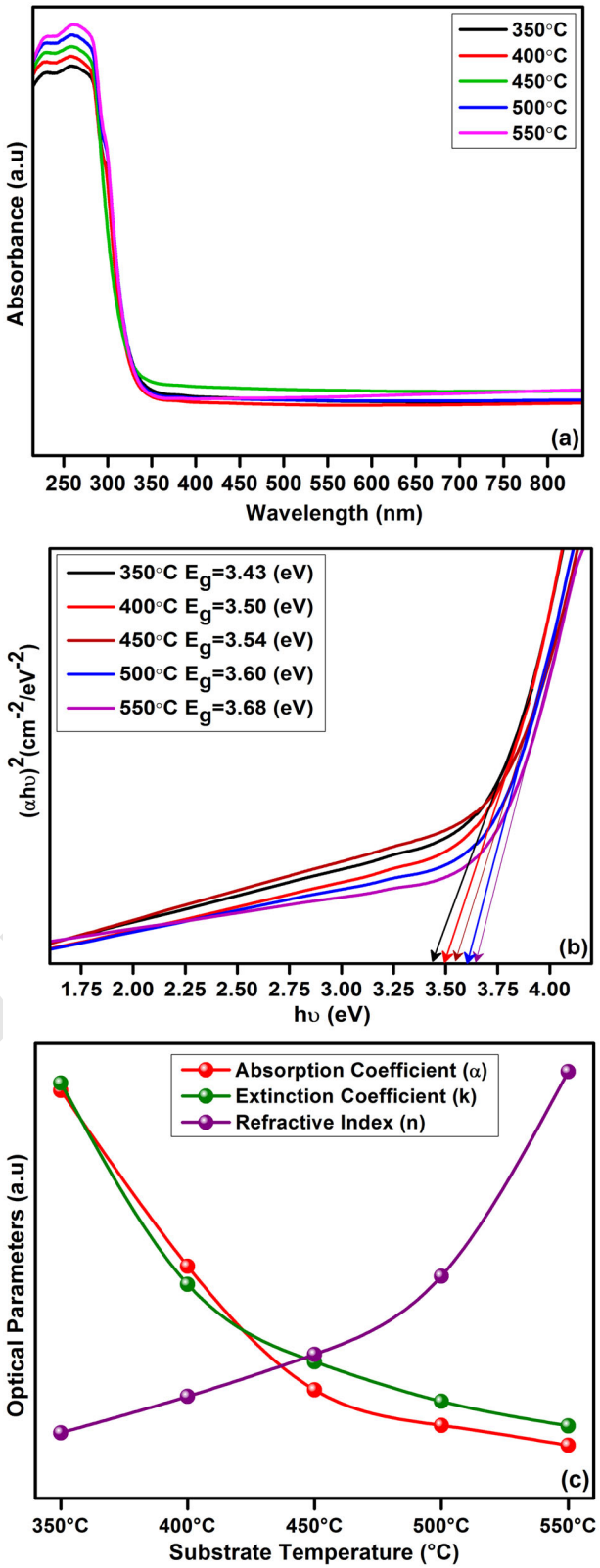


Fig. 8 **a** Absorbance Spectra for Yb_2O_3 thin films obtained at different substrate temperatures. **b** Plots of $(\alpha h\nu)^2$ vs $h\nu$ for Yb_2O_3 thin films obtained at different substrate temperatures. **c** Optical Parameters for Yb_2O_3 thin films obtained at different substrate temperatures

UNCORRECTED

Table 4 Optical parameters of Yb_2O_3 thin films with different substrate temperature

Substrate temperature (°C)	Absorption coefficient (α) $(cm)^{-1}$	Extinction coefficient (k)	Refractive index (n)	Band gap (eV)
350	6.62×10^6	0.221	2.792	3.43
400	6.31×10^6	0.203	2.797	3.50
450	6.09×10^6	0.197	2.805	3.54
500	6.03×10^6	0.193	2.819	3.60
550	5.99×10^6	0.191	2.855	3.68

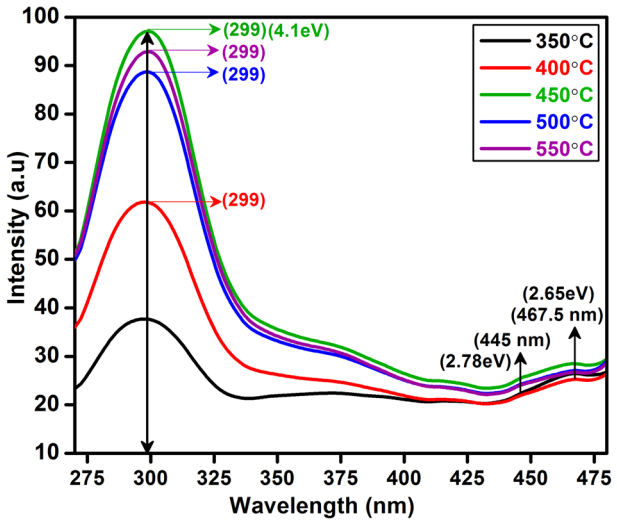


Fig. 9 PL measurements of Yb_2O_3 thin films coated at various substrate temperatures

fabricated at 450 °C. In addition, the Yb_2O_3 thin films have three PL emission peaks near 372 nm, 445 nm, and 468 nm [43]. The spectra show that strong emission bands are evident for the films prepared at temperatures of 450 to 550 °C when compared to the other films, demonstrating that these samples are potentially suitable for use in semiconductor device applications.

3.8 Electrical conductivity

Figure 10(a–e) shows the dc electrical conductivity of the Yb_2O_3 thin films at different substrate temperatures using a two-probe setup as the temperature of the device varies from 30 °C to150 °C. If the applied voltage is varied from 10 to 100 V, the current value of all the samples was observed to rise linearly. It is observed that this trend is similar at all temperatures from room temperature to 150 °C. The maximum current value is obtained for the higher device temperature at 150 °C. The conductivity σ at room temperature is calculated using the following relation (11), [44] which shows that there is an increase in the conductivity with an increase in the substrate temperature and their values are listed in Table 5 and Fig. 11.

$$\text{Electrical Conductivity} \qquad (\sigma_{dc}) = \frac{t}{RA} \qquad (11)$$

where t is the thickness of Yb_2O_3 film, R is the resistance of the film and A is the active area of the film. This behavior is due to an increase in the grain size in the film, which varies with the rise in temperature. In addition, the reduction of the grain boundary values in the Yb_2O_3 thin films due to the shorter diffusion length of the hole can also enhance the lifetime of the charge carriers. The semiconducting nature of Yb_2O_3 thin films is verified by this conductivity property. It is apparent that the electrical properties of Yb_2O_3 thin films can be enhanced by modifying the temperature of the substrate. The activation energy is calculated using relation 12.

$$\text{Activation Energy} \qquad (\sigma) = \sigma_0 \exp\left(\frac{-E_a}{k_B T}\right) \qquad (12)$$

where σ_0, k_B, E_a are the pre-exponential factor, Boltzmann constant, and activation energy, respectively. From the above relation (12), the minimum average activation energy of 0.395 eV is obtained for Yb_2O_3 film at 550 °C as shown in Table 5. The reduction in the activation energy at higher substrate temperatures is due to the transition of thermally triggered electrons from the valence band to the conduction band without any defects or traps. Figure 12 exhibits substrate temperature versus average conductivity and activation energy of Yb_2O_3 thin films. The average conductivity increases with increasing substrate temperature, which is due to the increase in the grain size of Yb_2O_3 thin films. From Fig. 12, we observe that the average activation energy decreases with an increasing substrate temperature of Yb_2O_3 thin films.

3.9 J−V characteristics of Al/Yb_2O_3/p-Si Schottky barrier diode

Temperature-dependent I-V characterization is the most effective way of calculating electrical parameters (n and Φ_B) of MS and MIS structured SBDs. The Al/Yb_2O_3/p-Si SBDs were fabricated at various substrate temperatures from

UNCORRECTED PROOF

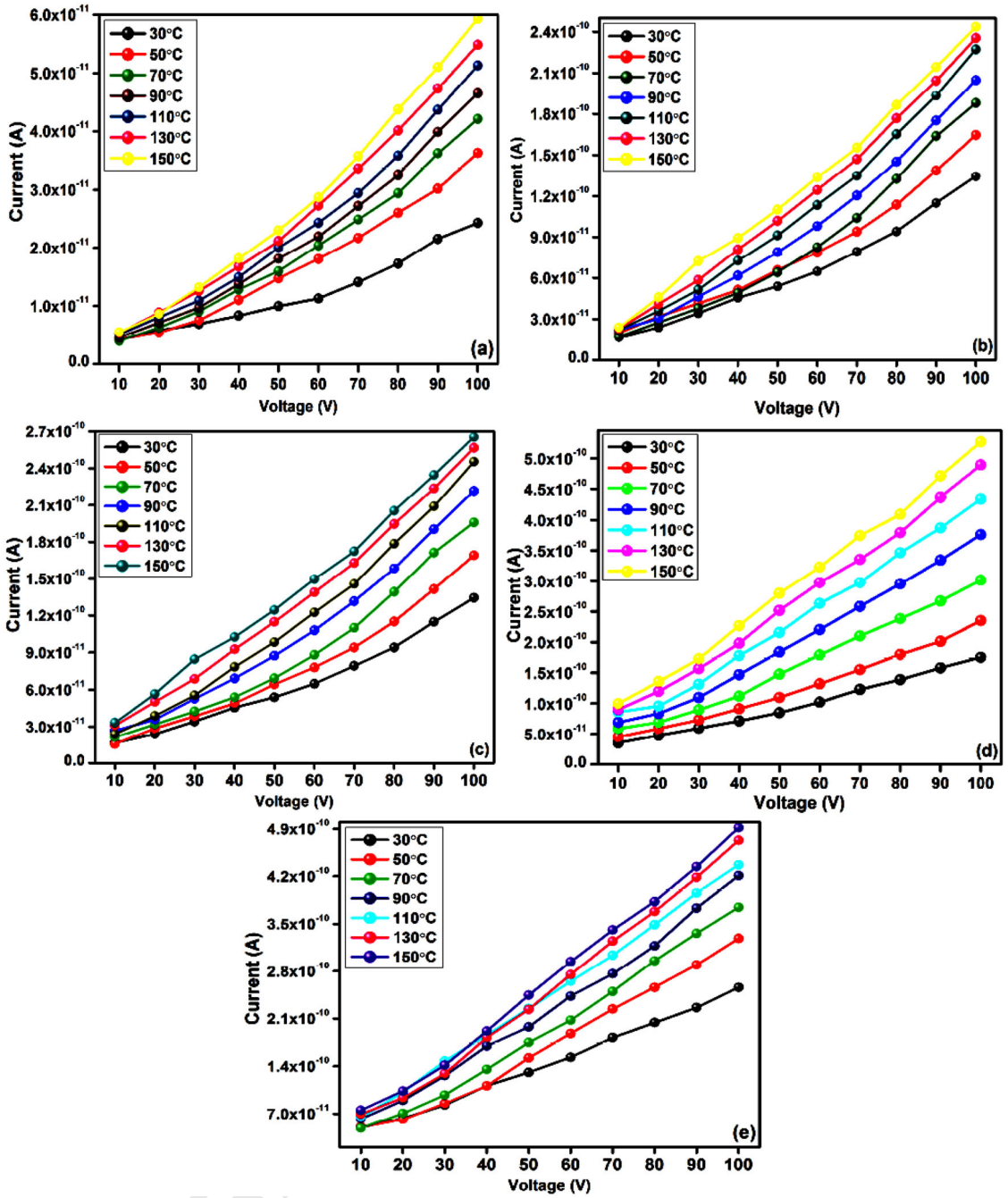


Fig. 10 Temperature-dependent current-voltage characteristics of Yb_2O_3 thin films obtained at different T_{sub} of **a** 350 °C, **b** 400 °C, **c** 450 °C, **d** 500 °C, and **e** 550 °C

350 °C to 550 °C. In dark and light conditions, forward and reverse current values of the MIS structure SBDs are measured at different unit temperatures (30, 50, 70, 90, 110, 130, and 150 °C) by applying a bias voltage of –3 to +3 V (in 0.3 V steps), as shown in Fig. 13(a–e). The charge transport mechanism between the Al/Yb_2O_3/p-Si SBD interfaces is explained by the principle of thermionic emission (TE), for which the state is $V > 3K_BT/q$. The saturation current density ($J = I/A$) of the Al/Yb_2O_3/p-Si SBDs can be determined using the following Eqs. (13, 14), according to TE theory [45].

$$\text{Current Density} \quad (J) = J_0 \exp\left(\frac{qV}{nK_{BT}} - 1\right) \tag{13}$$

$$\text{Reverse Saturation Current} \quad (I_0) = J_0/A = A^*T^2 \exp\left(-\frac{q\phi_B}{K_BT}\right) \tag{14}$$

Table 5 Electrical parameters of Yb_2O_3 thin films for various substrate temperatures

Substrate Temperature (°C)	Average Conductivity ($S\ cm^{-1}$)	Activation energy (eV)
350	4.33×10^{-16}	0.449
400	1.20×10^{-15}	0.442
450	1.81×10^{-15}	0.423
500	2.42×10^{-15}	0.402
550	3.06×10^{-15}	0.395

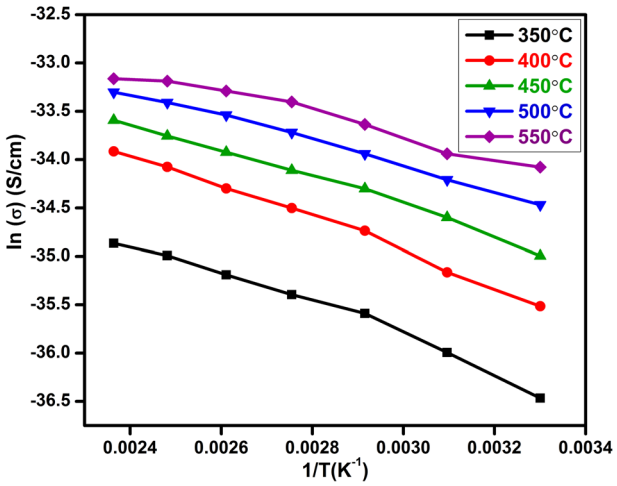


Fig. 11 Plot of ln (σ) vs. 1/T for Yb_2O_3 thin films obtained at a different substrate temperature

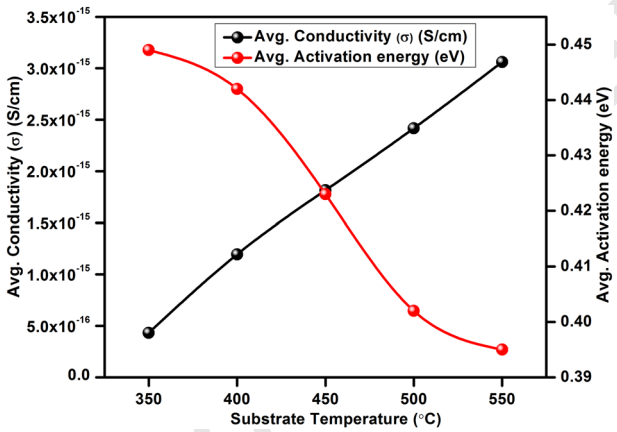


Fig. 12 Electrical parameters vs. Substrate temperature for Yb_2O_3 thin films

where J_0 is the reverse leakage current density, q is the electron charge, V is the applied voltage (10–100), n is the ideality factor of the device, K_B is the Boltzmann constant value (1.3807×10^{-23} J.K^{-1}), T is the absolute temperature and A* is the effective Richardson constant for p-type Si wafer (A* = 32 A/cm^{2}k^{-2}). The highest current values for higher system temperature (150 °C) are seen by all SBDs with good rectification behavior. The observed I_o values in dark condition varied from 1.82×10^{-5} A to 1.99×10^{-6} A, which was found to be improved in light condition from 3.39×10^{-4} A to 8.55×10^{-5} A (all values are listed in Table 6). The findings obtained indicate that the device performance and σ values of the Al/ Yb_2O_3/p-Si diodes are enhanced due to the rise in the number of electron-hole pairs with the rising voltage at higher temperatures. In addition, the current depends on the tunneling probability exp $(-a(\delta X)^{1/2})$ via an interface layer, and the current increases with the mean tunneling barrier reduced [46]. The semi-logarithmic plot of current density (InJ) versus voltage (V) is shown in Fig. 14(a–e). The ideality factor of the MIS structure SBDs is determined from the slope and the intercepts of the semi-logarithmic forward bias of the J-V plot for the condition $V > 3K_BT/q$. The ideality factor (n) and barrier height (Φ_B) can be determined by the following relations (15, 16) [47] and are summarized in Table 6.

$$\text{Ideality factor} \qquad (n) = \frac{q}{k_B T}\left(\frac{d(V)}{d(\ln(J))}\right) \tag{15}$$

$$\text{Barrier height} \qquad (\Phi_B) = \frac{k_B T}{q}\ln\left(\frac{AA^* T^2}{I_0}\right) \tag{16}$$

while ideality factor values have decreased from 5.042 to 2.537 and 4.205 to 2.059 under dark and light conditions, respectively, with increased substrate temperature, the barrier height (Φ_B) was also found to increase gradually under the dark and light condition at higher substrate temperature. The barrier height (Φ_B) attained in dark conditions increases from 0.678 to 0.789 eV and 0.602 to 0.638 eV under the light as substrate temperature increases. The obtained ideality factors are slightly higher compared to an ideal diode, which is usually equal to unity. However, most of the time, metal-semiconductor device has high ideality factors. With decreased interfacial layer thickness and the mean tunneling barrier, the barrier height is observed to increase [48]. The obtained higher ideality factor attributes to barrier inhomogeneity, non-uniform distribution of the carriers in the interfaces, interface state, the tunneling process, and image force effects [49]. In addition, the higher ideality factor may be related to the recombination of electrons and holes in the depletion region, current mechanism due to a large number of surface states, or diffusion current [50]. In this investigation, the higher ideality factor values may be associated with the interface state, the presence of a thin native oxide layer (SiO_2) between the MS junction, and the formation of a barrier inhomogeneity due to the interfacial Yb_2O_3 layer [51]. When the device is exposed to the light it strays from

UNCORRECTED PROOF

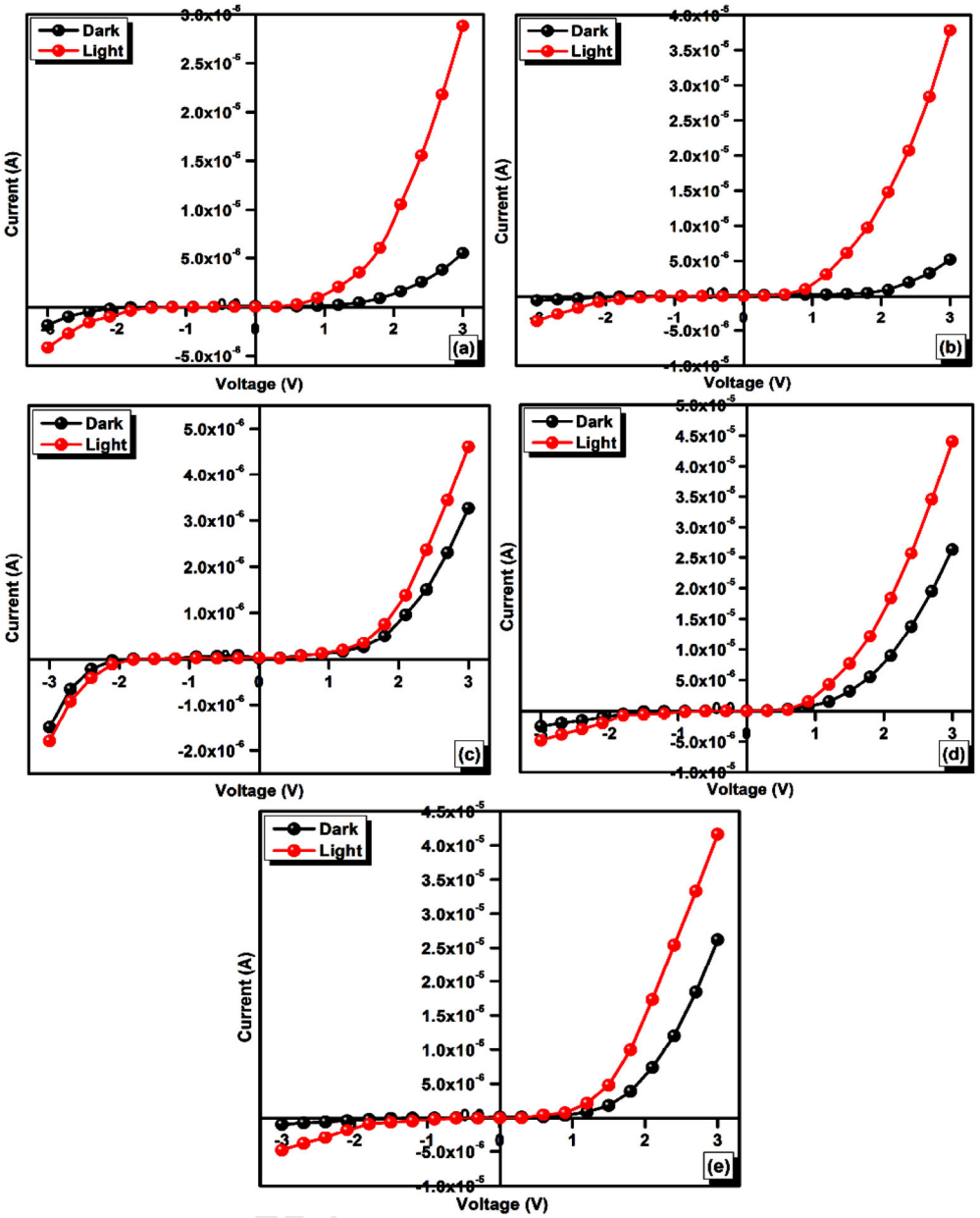


Fig. 13 I-V characteristics of Al/Yb_2O_3/p-Si Schottky barrier diode for various substrate temperatures of **a** 350 °C, **b** 400 °C, **c** 450 °C, **d** 500 °C, and **e** 550 °C

Table 6 Electrical parameters of Al/Yb_2O_3/p-Si (MIS) Schottky Diodes with different substrate temperature

Substrate Temperature (°C)	J–V Method					
	Ideality factor (*n*)		Barrier Height (ΦB) (eV)		Saturation current density (Jo)	
	Dark	Light	Dark	Light	Dark	Light
350	5.042	4.205	0.678	0.602	1.82×10^{-05}	3.39×10^{-04}
400	4.833	3.821	0.681	0.611	1.61×10^{-05}	2.38×10^{-04}
450	4.394	3.219	0.705	0.623	6.44×10^{-06}	1.52×10^{-04}
500	3.586	2.464	0.736	0.631	2.65×10^{-06}	1.10×10^{-04}
550	2.537	2.059	0.789	0.638	1.99×10^{-06}	8.55×10^{-05}

UNCORRECTED

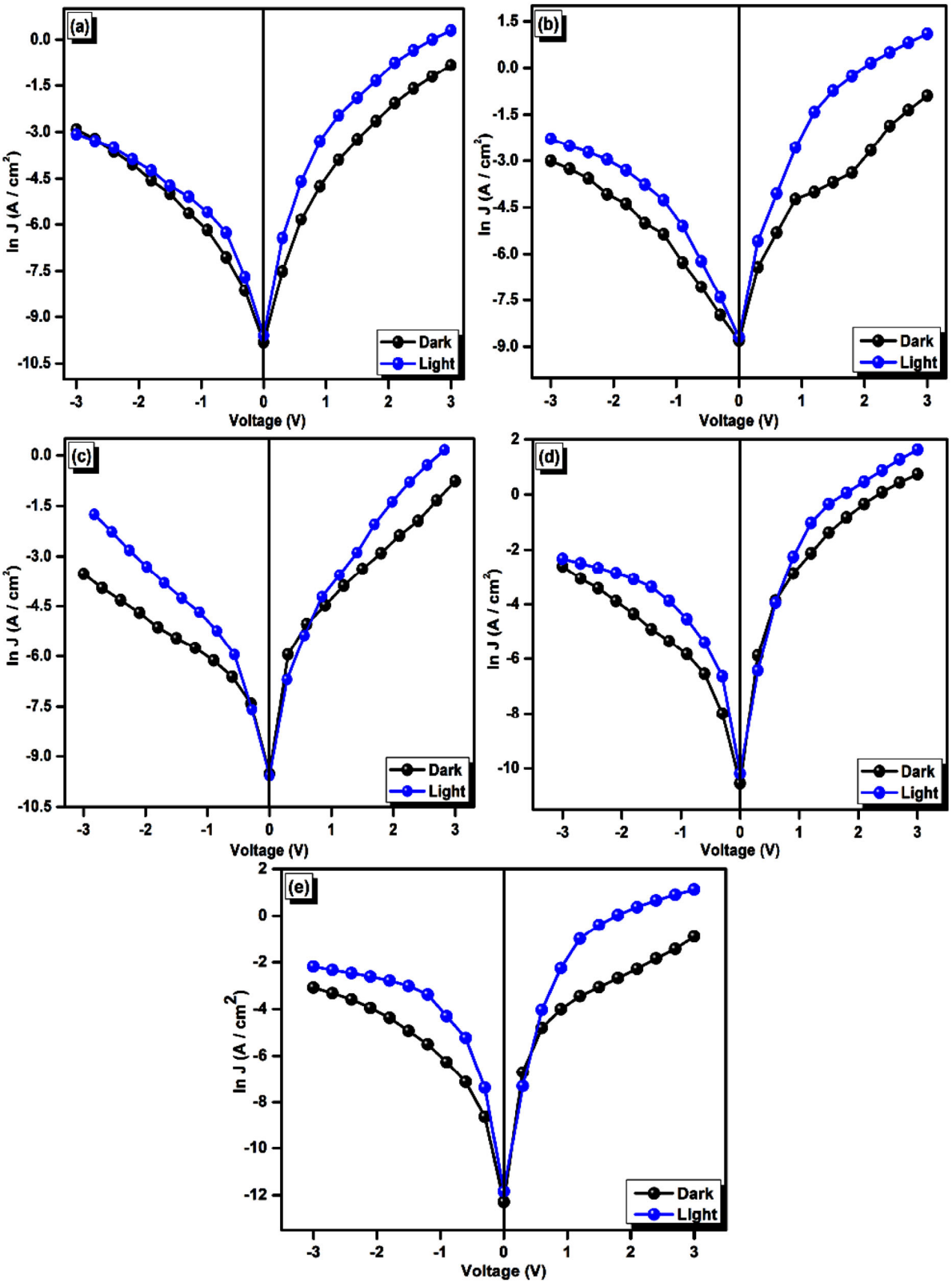


Fig. 14 Semi Logarithmic Plot of ln (J) vs. V for Al/Yb_2O_3/p-Si SBDs for various T_{sub} of **a** 350 °C, **b** 400 °C, **c** 450 °C, **d** 500 °C, and **e** 550 °C

ideality because of increasing carrier concentration at the interface [52]. The findings indicate that the MIS structured SBDs prepared at 550 °C under dark and light conditions offer a minimum n equal to 2.537 & 2.059 and Φ_B equal to 0.789 eV & 0.638 eV which would offer more rectification behavior and greater thermal stability of the system than at other substrate temperatures [53].

4 Conclusion

We have successfully fabricated Al/Yb_2O_3/p-Si (MIS) SBDs by maintaining substrates at various temperatures. XRD analysis indicates that the entireYb_2O_3 films exhibit a single crystalline structure together with a cubic structure. The D_{avg} value attains a maximum value at a higher substrate temperature of 550 °C. A cage-like structure over the entire surface of the substrate is recorded in the FESEM image. The elemental composition spectrum confirms the presence of Yb and O. The UV-Visible spectra show a maximum bandgap energy (Eg = 3.68 eV) for the Yb_2O_3 thin films deposited at 550 °C. The topographic study exhibits a greater surface roughness and RMS values for the sample prepared at higher substrate temperature. The PL spectra of Yb_2O_3 thin films indicate strong and broad emission bands at 299 nm. The I-V characteristics of the Yb_2O_3 thin film at 550 °C reveal a higher electrical conductivity (σ_{dc}) of 3.06×10^{-5} S/cm and minimum activation energy of 0.395 eV. From the diode results, all the Al/Yb_2O_3/p-Si structured SBDs indicate a strong +ve photoconductive response. Notably, the MIS structure SBDs prepared at 550 °C display a lowest (n) value of 2.537 and 2.059 with corresponding Φ_B value of 0.789 eV and 0.638 eV under dark and light conditions, respectively. Thus, the current work resulted in the fabrication of a device based on novel rare earth interfacial layer that can be used in many high-speed switching device applications in optoelectronics and microelectronics industries.

Publisher's note Springer Nature remains neutral with regard to jurisdictional claims in published maps and institutional affiliations.

References

1. Kang H-S, Reddy MSP, Kim DS, Kim KW, Ha JB, Lee YS, Choi HC, Lee JH (2013) J Phys D: Appl Phys 46:155101-1–15155106
2. Pearton SJ, Ren F, Zhang AP, Dang G, Cao XA, Lee KP, Cho H, Gila BP, Johnson JW, Monier C, Abernathy CR, Han J, Baca AG, Chyi JI, Lee CM, Nee TE, Chuo CC, Chu SNG (2001) Mater Sci Eng B 82:227–231
3. Orak, Kocyigit A, Turut A (2017) J Alloys Compd 691:873–879
4. Simchi H, Heidarisaani M, Esmaeilzadeh M AIP Adv 3:032124
5. Xia P, Feng X, Ng RJ, Wang S, Chi D, Li C, He Z, Liu X, Ang K-W (2017) Sci Rep 7:40669
6. Demircioglu O, Karatas S, Yıldırım N, Bakkaloglu OF, Turut A (2011) J Alloys Compd 509: 6433–6439
7. Ejderha K, Duman S, Nuhoglu C, Urhan F, Turut A (2014) J Appl Phys 116:234503
8. Yıldırım M, Kocyigit A (2018) J Alloys Compd
9. Pan T-M, Cheng C-H, Lee C-D (2009) J Electrochem Soc 156: J108-J111
10. Scarel G, Svane A, Fanciulli M (2006) Top AppL Phys 106(2):1–14
11. Liu, Liu GX, Zhu HH, Xu F, Fortunato E, Martins R, Shan FK (2014) ACS Appl Mater Interfaces 6:17364–17369
12. Esro M, Kolosov O, Stolojan V, Jones PJ, Milne WI, Adamopoulos G (2017) Adv Electron Mater 3:1700025
13. Ben Farhat L, Amami M, Hlil EK, Ben R Hassen (2010) Mater Res Bull 45:1964–1968
14. Pan Tung-Ming, Chen Ching-Hung, Chen Fa-Hsyang, Huang Yu-Shu, Her Jim-Long (2015) J Disp Technol 11(3):248–254.
15. Rajagopal Reddy V, Dasaradha Rao V, Janardhanam V, Kang M-S, Choi C-J (2013) Mater Transac 54(12):2173–2179.
16. Jyothi I, Janardhanam V, Kim J-H, Yun H-J, Jeong J-C, Hong H, Lee SN, Choi CJ (2016) J Alloys Compd 07:292
17. Marnadu R, Chandrasekaran J, Vivek P, Balasubramani V, Maruthamuthu S (2020) Zeitschrift für Physikalische Chemie 234 (2):355–379.
18. Vivek P, Chandrasekaran J, Marnadu R, Maruthamuthu S, Balasubramani V (2019) Superlattices Microstructures 133:106197
19. Marnadu R, Chandrasekaran J, Raja M, Balaji M, Maruthamuthu S, Balraju P (2018) Superlattices Microstructures 119:134
20. Ramana CV, Utsunomiya S, Ewing RC, Julien CM, Becker U (2006) J Phys Chem B110:10430
21. Balasubramani, Chandrasekaran J, Marnadu R, Vivek P, Maruthamuthu S, Rajesh S (2019) J Inorg Organomat Polymers Mater
22. Pan T-M, Huang W-S (2009) Appl Surf Sci 255:4979–4982
23. Wiktorczyk T, Wesolowska C (1980) Thin Solid Films 37 (1–2):107–109
24. Malvestuto M, Scarel G, Wiemer C, Fanciulli M, Acapito F D', Boscherii F, X (2006) Nucl Instr Meth Phys Res B 246:90–95
25. Oh I-K, Kim K, Lee Z, Ko KY, Lee C-W, Lee S-J, Myung JM, Lansalot-Matras C, Noh W, Dussarrat C, Kim H, Lee H-B-R (2015) Chem Mater 27:148–156
26. Spiga S, Wiemer C, Scarel G, Costa O, Marco, Fanciulli M (2007) Top Appl Phys 106:203–223
27. Marnadu R, Chandrasekaran, Raja M, Balaji M, Balasubramani V (2018) J Mater Sci: Mater Electronics 29:2618–2627
28. Sumathi P, Chandrasekaran J, Marnadu R, Muthukrishnan S, Maruthamuthu S (2018) J Mater Sci: Mater Electronics 10854-018-9776-7
29. Mohan KS, Panneerselvam A, Chandrasekaran J, Marnadu R, Shkir Mohd. (2021) Appl Nanosci 11:1617–1635
30. Petroff P, Sheng TT, Sinha AK, Rozgonyi GA, Alexander FB (1973) J Appl Phys 44:2545
31. Qian C, Tianmei Z, Hongrong L (2013) Adv Condens Matter Phys 2013: 519869
32. Balaji M, Chandrasekaran J, Raja M (2016) Mater Sci Semiconductor Process 43:104–113
33. Titov, Sokolova NP, Vorob'eva MV, Opolchenova NL, Eremenko ZV, Stepareva NN (2009) Inorg Mater 45(8):884–888. ISSN 0020-1685
34. Henriques MS, Ferreira AC, Cru A, Ferreira LM, Branco JB, Brázda P, Jurek K, Stora T, Gonçalves AP (2015) Ceram Int 41:10795–10802
35. Suresh R, Ponnuswamy V, Sankar C, Manickam M, Mariappan M (2016) RSC Adv 6:53967–53980.
36. Lobaccaro P, Raygani A, Oriani A, Miani N, Piotto A, Kapadia R, Zheng M, Yu Z, Magagnin L, Chrzan DC, Maboudian R, Javey A (2014) J Electrochemical Soc 161(14):D794–D800

UNCORRECTED PROOF

37. Mohanraj K, Balasubramanian D, Chandrasekaran J (2018) J Alloys Compd, https://doi.org/10.1016/j.jallcom.2018.11.264
38. Ohmi S, Kobayashi ZC, Kashiwagi I, Ohshima C, Ishiwara H, Iwai H (2003) J Electrochemical Soc 150(7):F134–F140
39. Akhtar MJ, Alhadlaq HA, Alshamsan A, Khan MAM (2015) Sci Rep 5:13876
40. Kahraman A, Karacali H, Yilmaz E (2020) J Alloys Compd 825:154171
41. Suresh R, Ponnuswamy V, Mariappan R, Senthilkumar N (2014) Ceram Int 40:437–445
42. Muralidharan M, Sivakumar K, Sivaji K (2018) Mechanics, Mater Sci Eng 15. ISSN 2412-5954
43. Vivek P, Chandrasekaran J, Marnadu R, Maruthamuthu S, Balasubramani V (2019) Superlattices Microstruct 133:106197.
44. Guo W, Hao H, Jin S, Su Q, Li H, Hu X, Gan Y, Qin L, Gao W, Liu G (2016) Ceram Int 12:077
45. Alfaramavi K (2008) Optoelectronics Adv Mater – Rapid Commun 2:763–765
46. Raja M, Chandrasekaran J, Balaji M, Janarthanan B (2016) Mater Sci Semicond Process 56:145
47. Ravinandan M, Koteswara Rao Peta, Rajagopal Reddy V (2009) Semicond Sci Technol 24:035004
48. Rajagopal Reddy V, Sri Silpa D, Janardhanam V, Yun HJ (2015) Electron Matter Lett 11(1):73–81
49. Katsuno T, Watanabe Y, Fujiwara H, Konishi M, Naruoka H, Morimoto J, Morino T (2011) T Endo Appl Phys Lett 98:222111
50. Mohan KS, Panneerselvam A, Marnadu R, Chandrasekaran J, Shkir Mohd., Tataroğlu A (2021) Inorg Chem Commun 129:108646.
51. Qasrawi AF, Zakarneh YA, Gasanly NM (2017) IEEE Sensors J 17(14)
52. Mahesha MG, Kasturi VB, Shivakumar GK (2008) Turkish J Phys 32(3):151–156
53. Tataroglu A, Altındal S (2008) Microelectronic Eng 85:1866–1871

UNCORRECTED PROOF

Journal : **10971**
Article : **5683**

Springer
the language of science

Author Query Form

Please ensure you fill out your response to the queries raised below and return this form along with your corrections

Dear Author

During the process of typesetting your article, the following queries have arisen. Please check your typeset proof carefully against the queries listed below and mark the necessary changes either directly on the proof/online grid or in the 'Author's response' area provided below

Queries	Details Required	Author's Response
AQ1	Note that the eproof should be amended in only one browser window at any one time; otherwise changes will be overwritten.	
AQ2	You cannot alter accepted Supplementary Information files except for critical changes to scientific content. If you do resupply any files, please also provide a brief (but complete) list of changes. If these are not considered scientific changes, any altered Supplementary files will not be used, only the originally accepted version will be published.	
AQ3	Author surnames have been highlighted. Please check these carefully and adjust if the first name or surname is marked up incorrectly. Note that changes here will affect indexing of your article in public repositories such as PubMed. Also, carefully check the spelling and numbering of all author names and affiliations, and the corresponding email address(es).	
AQ4	Please check your article carefully, coordinate with any co-authors and enter all final edits clearly in the eproof, remembering to save frequently. Once corrections are submitted, we cannot routinely make further changes to the article.	
AQ5	Please provide page range in the Reference number [51]	
AQ6	Please provide complete bibliographic details in Reference number [4].	
AQ7	Please provide page range and volume number in Reference number [8,21]	
AQ8	Please check and confirm the author name(s) in Reference number [52].	
AQ9	Please provide 'Competing Interests' statement.	

UNCORRECTED PROOF